Open access • Journal Article • DOI:10.1021/ACS.EST.9B05728

Spatially Resolved Localization of Lanthanum and Cerium in the Rare Earth Element Hyperaccumulator Fern Dicranopteris linearis from China. — Source link

Wen-Shen Liu, Antony van der Ent, Antony van der Ent, Peter D. Erskine ...+7 more authors

Institutions: Sun Yat-sen University, University of Queensland, University of Lorraine

Published on: 17 Jan 2020 - Environmental Science & Technology (American Chemical Society)

Topics: Dicranopteris linearis and Fern

Contaminants in Aquatic and Terrestrial Environments

Spatially-resolved localization of lanthanum and cerium in the rare earth element hyperaccumulator fern Dicranopteris linearis from China

Wenshen Liu, Antony van der Ent, Peter D. Erskine, Jean-Louis Morel, Guillaume Echevarria, Kathryn M. Spiers, Emmanuelle Sophie Montarges-Pelletier, Rong-Liang Qiu, and Ye-Tao Tang

Environ. Sci. Technol., **Just Accepted Manuscript** • DOI: 10.1021/acs.est.9b05728 • Publication Date (Web): 17 Jan 2020

Spatially-resolved localization of lanthanum and cerium in the rare earth element hyperaccumulator fern *Dicranopteris linearis* from China

Wen-Shen Liu[1,2,3], Antony van der Ent[4,5], Peter D. Erskine[4], Jean Louis Morel[5], Guillaume Echevarria[4,5], Kathryn M. Spiers[6], Emmanuelle Montargès-Pelletier[7], Rong-Liang Qiu[1,2,3], Ye-Tao Tang[1,2,3,*]

[1]School of Environmental Science and Engineering, Sun Yat-sen University, Guangzhou 510275, China.

[2]Guangdong Provincial Key Laboratory of Environmental Pollution Control and Remediation Technology, Sun Yat-sen University, Guangzhou 510275, China.

[3]Guangdong Provincial Engineering Research Center for Heavy Metal Contaminated Soil Remediation, Sun Yat-sen University, Guangzhou 510275, China.

[4]Centre for Mined Land Rehabilitation, Sustainable Minerals Institute, The University of Queensland, St Lucia, Queensland 4072, Australia.

[5]Université de Lorraine, INRA, Laboratoire Sols et Environnement, Nancy 54000, France.

[6]Photon Science, Deutsches Elektronen-Synchrotron DESY, Hamburg 22607, Germany.

[7]CNRS – Université de Lorraine Laboratoire Interdisciplinaire des Environnements Continentaux, Vandoeuvre-lès-Nancy F-54500, France.

* **Corresponding author**

Address: School of Environmental Science and Engineering, Sun Yat-sen University, Guangzhou 510275, China

E-mail: eestyt@mail.sysu.edu.cn

Tel/Fax. +86-020-39332743

GRAPHIC ABSTRACT

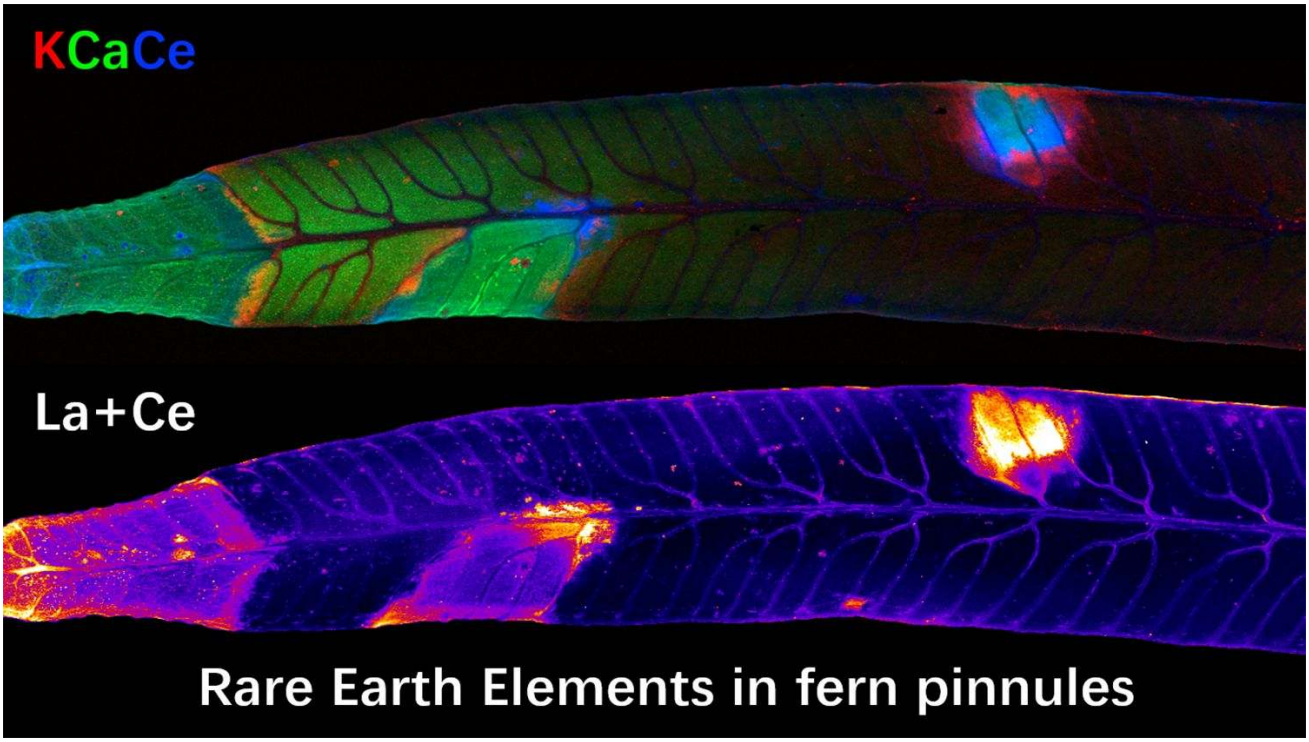

ABSTRACT

The fern *Dicranopteris linearis* (Gleicheniaceae) from China is a hyperaccumulator of Rare Earth Element (REE), but little is known about the ecophysiology of REE in this species. This study aimed to clarify tissue-level and organ-level distribution of REEs *via* synchrotron-based X-ray fluorescence microscopy (XFM). The results show that REEs (La + Ce) are mainly co-localised with Mn in the pinnae and pinnules, with the highest concentrations in necrotic lesions and lower concentrations in veins. In the cross-sections of the pinnules, midveins, rachis and stolons La + Ce and Mn are enriched in the epidermis, vascular bundles, and pericycle (midvein). In these tissues, Mn is localised mainly in the cortex and mesophyll. We hypothesize that movement of REEs in the transpiration flow in the veins is initially restricted in the veins by the pericycle between vascular bundle and cortex, whilst excess REEs are transported by evaporation and co-compartmentalized with Mn in the necrotic lesions and epidermis in an immobile form, possibly a Si-coprecipitate. The results presented here provide insights in how *D. linearis* regulates high concentrations of REEs *in vivo*, and this knowledge is useful for developing phytotechnological applications (such as REE agromining) using this fern in REE-contaminated sites in China.

Key words: X-ray fluorescence microscopy; compartmentalization; necrosis; vein; manganese; silicon.

INTRODUCTION

Rare earth elements (REEs), which include 15 lanthanides and yttrium (Y), have a range of applications in modern technologies, such as high-strength magnets, electric vehicles and medical devices, and increasing demand for these technologies has resulted in a growing need for REEs (1). Consequently, mining activities and a subsequent release of wastes into the environment, may pose a threat to agricultural crops and ultimately human health (2).

Some REEs can be beneficial to plants at low concentrations (3) yet can be toxic to plants at higher concentrations (4). However, hyperaccumulator plants are able to accumulate and tolerate high concentrations of potentially toxic elements in their living shoots (5–7). Thus far ~700 plant species have been reported globally to hyperaccumulate a large variety of metals and metalloids (8), but only 22 plant species are currently recognized as REE (hyper)accumulators (9, 10). These hyperaccumulator plants potentially offer an environmentally-friendly and cost-effective option for phytoremediation of REE polluted soils and recovery of REEs from low-grade ores and mining wastes (11). In this scenario, knowledge on the ecophysiology of REE hyperaccumulator plants is important to better understand the mechanisms for uptake, translocation and sequestration of REEs into living shoots. To date, most studies have focused on the uptake of nickel (Ni), zinc (Zn), cadmium (Cd) and arsenic (As) in various hyperaccumulator plant models (12–15), while much less is known about the ecophysiology of REE hyperaccumulator plants (16).

Elucidating the spatial distribution of metal(loid)s and their associations with other elements is key to understanding the mechanisms of tolerance in hyperaccumulator plants (17, 18). Over the past decades, elemental distribution in tissues, cells and organelles of a selection of hyperaccumulator plants have been studied extensively (18). Excess metal(loid)s are typically concentrated in bio-inactive tissues of the leaves to minimize the damage to biological activities (17). This includes Ni localised in foliar epidermal cells, vascular tissues and basal parts of trichomes of *Alyssum murale* (12), Zn in the vascular and epidermal cells of *Sedum alfredii* and *Sedum plumbizincicola* (13, 14), and As in the venules and the edges of the pinnae of *Pteris vittata* (15). Meanwhile, vacuole compartmentalization is thought to be a key component of metal(loid)s detoxification in leaves (19). Except for cerium (Ce) (+3 and +4 valences) and europium (Eu) (+2 and +3 valences), the REEs are a group of trivalent elements which show biochemical behavior that differs from other metals *e.g.* higher affinity to O-containing ligands but lower affinity to S-/N-containing ligands than Zn, Ni, Cd, *etc*. (20). Thus, REE in hyperaccumulators may have distinct uptake and transport mechanisms that are yet to be fully understood.

Dicranopteris linearis of the Gleicheniaceae family (synonym *D. dichotoma*)) is a native pioneer fern common throughout the Old World (sub)tropics and Oceania (USDA, GRIN-Taxonomy), and a dominant species grown on ion-adsorption REE mine tailings in Sothern China (Fig. S1). This species can grow in acidic (pH 4–5) and poor soils, and exhibits high phosphorus use efficiency (21, 22). To date, only the *D. linearis* accessions from Southern China have been recognized as a REE hyperaccumulator (10). Field surveys confirm that *D. linearis* can accumulate up to 0.2% REEs in

the aboveground parts when growing on REE mine tailings (Table S1). In the roots of *D. linearis*, REE deposits are found in the cell wall, intercellular space, plasmalemma, vesicles, and vacuoles of the endodermis by scanning electron microscopy with energy-dispersive spectroscopy (23), while in the pinnae, most of the REEs are thought to be accumulated in the cell walls, as shown by differential extractions of *D. linearis* tissue (24). Overall, the different techniques and samples preparations used to unravel those different observations have led to some insights, but we are far from fully understanding the ecophysiological mechanisms underlying the tolerance of *D. linearis* to high concentrations of REEs inside its living fronds.

Synchrotron-based X-ray fluorescence microscopy (XFM) is a non-destructive method that has been successfully used to study the *in-situ* distribution of trace elements in numerous hyperaccumulator plants (18, 25) and also in crop plants (26, 27). The aim of this study was to better understand the ecophysiological mechanisms that enable tolerance to high *in vivo* concentrations of REEs in this fern. To that end, XFM elemental images of the sum of two light REEs (*e.g.* the sum of La and Ce) and of K, Ca and Mn inside various *D. linearis* tissues were acquired.

MATERIALS AND METHODS

Collection of plant and soil samples. Live samples of *D. linearis* grown on the ion-adsorption REE mine tailings of Ganzhou, Jiangxi Province, China (24°57′N, 115°05′E) were collected. The REE mine tailings in this region occupied an area of >100 km^2, the soils of which are featured with low concentrations of nutrients (*e.g.* phosphorus) and organic matter (<0.1%), but high prevailing

concentrations of REEs (409–1035 mg kg^{-1}) and acidity (pH ~4) (28). Three mature plants with rhizosphere soil were brought alive to the P06 beamline (PETRA III Synchrotron, DESY, Hamburg, Germany) for the experiments described below. In parallel, four mature live pinnae and three dead standing litter of pinnae (the dead pinnae were still connected to the stolon) samples from a *D. linearis* population on an ion-adsorption REE mine tailing were sampled for bulk chemical analysis (Fig. S2). In order to investigate the accumulation characteristics of REE in *D. linearis* growing on REE mine tailings, plant and the corresponding rhizosphere soil samples from REE mine tailings (MT), edge of REE mine tailings (TE), non-mine area near REE mine tailings (NM), low/high levels of REE background regions (LB and HB) were collected (Table S1).

Chemical analysis of plant and soil samples. Plant samples were washed with deionized water (18Ω, 25°C), then dried in an oven at 105°C for 2 h and 60°C for 72 h. The analysis methods of total concentrations of Al, REEs, Si, and other nutrient elements (Mn, K, Ca, P) in pinna samples were adapted from Liu et al. (29). The analysis methods of REE in aboveground parts, underground parts and rhizosphere soil samples of *D. linearis* are shown in Table S1.

X-ray fluorescence microscopy (XFM). The X-ray fluorescence microscopy **(**XFM) experiment was undertaken at Beamline P06 at the PETRA III, a 6 GeV synchrotron (30). The undulator beam was monochromatized with a cryogenically cooled Si(111) channel-cut monochromator to an energy of 12 keV with a flux of 10^{10} photon/s. A Kirkpatrick-Baez mirror pair was used to focus the incident beam to 700 × 530 nm (hor × ver). The samples were scanned in fly-scan mode, with the resultant

131 sample X-ray signal detected using the Maia 384C detector system, operated in backscatter geometry
132 (31, 32). Typically, a quick 'survey scan' was first conducted to allow for the selection of the
133 appropriate portion of the sample. For the survey scan, the resolution was 50–100 μm with a dwell of
134 1–2 ms and generally took ca. 5 min to complete. After that a 'detailed scan' was conducted, with a
135 resolution of 2–10 μm and a dwell time of 15–20 ms. For the whole experiment, an incident energy
136 of 12.0 keV was used so that the fluorescence lines of the elements of interest were well below the
137 inelastic and elastic scatter peaks.
138
139 Hydrated pinnule samples were analysed whole, or as cross-sections which were hand cut with a
140 stainless-steel razor blade (employing a 'dry knife' method); whole or sectioned samples were then
141 immediately mounted between two sheets of 4 μm Ultralene thin film stretched over a 3D-printed
142 frame in a tight sandwich to limit evaporation, and analysed within 10 minutes after excision. The
143 possibility of radiation-induced damage in XFM analysis (especially in hydrated samples) is an
144 important consideration that may limit the information sought from the analysis (18). In a recent
145 study, radiation dose limits for XFM analysis were assessed, and in hydrated plant tissue dose-limits
146 are 4.1 kGy before detectable damage occurs (33). In order to limit radiation damage, we fast use
147 scanning by limiting per-pixel dwell time to < 20 ms.
148
149 **Data processing and statistics.** The XFM event stream was analysed using the Dynamic Analysis
150 method (34) as implemented in GeoPIXE (35). It was necessary to use a precise matrix file for the
151 spectra fitting to account for X-ray fluorescence absorption of the relatively low energy of the REEs

L-lines, and the matrix was based on the stoichiometry of the mean concentrations of major elements (limited to those present at >0.1 wt%) in dried *D. linearis* pinna samples (Table 1). The matrix composition assumed hydration of the fresh samples, and was formulated as $C_7O_{31}H_{59}N_{0.7}S_{0.2}Al_{0.3}Si_{1.5}Ca_{0.2}Mn_{0.1}K_{0.3}$ (on the basis of average concentrations of these elements in bulk samples) with a density of 0.90 g cm^{-3}, considering a covering and backing layer of Ultralene foil (4 μm), and considered to have a uniform thickness of 300 μm. The rhodium coating of the KB mirror focusing optics available for this experiment results in a high-energy cut-off of 23 keV, well below that required to excite the K-lines of the REEs (33.44 keV for La), so therefore the experiment had to rely on exciting the L-lines (ranging from 4.65 keV for La to 7.41 keV for Yb). The energy-resolution of the Maia 384C detector is ~220 eV and it is hence unable to distinguish between the numerous L-lines of the various REEs. Moreover, the L-lines of Nd, Gd, Eu and Sm are in the range of the K-lines of Mn and thus these elements, at low prevailing concentrations, are not possible to be distinguished reliably using the Maia detector. However, the Lα1-lines of La (4.65 keV) and Ce (4.84 keV) are sufficiently spectroscopy distinguishable and were used to represent the REEs. The only problematic line overlap that remains is the Nd Lβ2 line (~15% relative intensity) occurring at 6.087 KeV, while the Mn Kα1 line occurs at 5.900 KeV. Therefore, it makes a minor contribution to the Mn elemental maps, although this is near-negligible as the prevailing Mn concentrations are typically four-fold higher than those of Nd. Moreover, the fitting of the fluorescence spectra is not only dependent on the resolution of the detector, but also on the efficacy of the spectral fitting method. GeoPIXE generates a "Dynamic Analysis" matrix via a least-squares fit of an energy spectrum extracted from the scanned data from which elemental concentration maps are produced

from a matrix multiplication of the Dynamic Analysis matrix and the spectral data matrix for each pixel. This process effectively fits all spectral lines for identified elements and the resultant maps are inherently background subtracted and element overlap resolved.

Although Al and Si are implicated in REE accumulation and tolerance in *D. linearis* (16, 29), their K-lines are 1.47 and 1.74 keV respectively, and therefore could not be detected due to absorption of these low-energy X-rays in the air path between detector and sample.

RESULTS

Bulk elemental concentrations in *Dicranopteris linearis*. The bulk pinnae concentrations of REEs, Al, Si, Mn, K, Ca, and P are given in Table 1. The concentrations of Al, Si and REEs in live pinnae are around half that of the dead standing litter of pinnae – Al 2850 *vs* 4850 mg kg^{-1}, Si 14700 *vs* 33 900 mg kg^{-1} and REEs 1900 *vs* 3500 mg kg^{-1} respectively. The concentrations of Mn, P and K in live pinnae are always higher than the dead standing litter of pinnae – Mn 1480 *vs* 310 mg kg^{-1}, P 211 *vs* 129 mg kg^{-1} and K 3000 *vs* 268 mg kg^{-1} respectively. The concentration of Ca is not significantly different between the live or dead of pinnae. Among the 15 REEs, the sum of La and Ce accounts for ~50% of the total REEs in both the live and dead standing litter of pinnae fractions (Table 1; Table S2). As can be seen from Table S1, the REEs concentrations in the aboveground parts of *D. linearis* reach the highest at REE mine tailings (1470 ± 199 mg kg^{-1}), where the REEs concentrations in the rhizosphere soil are highest (518 ± 208 mg kg^{-1}). Meanwhile, the REE

accumulation factor (aboveground part/rhizosphere soil) is higher than 1 and there are no significant differences between these samples.

Localization of REEs in pinnae and pinnules. The X-ray fluorescence element maps reveal distinct distributions for K, Ca, Mn and the summed REEs (La + Ce) in the tissues of the pinnae (Fig. 1; Fig. S3) and the pinnules (Fig. 2; Fig. S4; Fig. S5) of *D. linearis*. The most significant enrichment of La + Ce and Mn occurs in the necrotic lesions, which are by definition the bio-inactive regions of the pinnae. The preferential accumulation of REEs in these necrotic spots appear in all of the tissue areas (pinna tips, margins and blades) where necrosis occurs. Significant La + Ce and Mn enrichments are also found in the midvein, secondary veins, tertiary veins and in the margins of the pinnae and pinnules. The distribution of La + Ce and Mn is not strictly restricted within the veins and necrotic lesions; as lower concentrations occur outside of the veins and necrotic lesions. Calcium is mainly distributed in the necrotic lesions and blade, but lower in the veins. Potassium has a distinctly different distribution in the pinnae and pinnules, and is mostly localised in the blade, and nearly absent in the necrotic lesions.

In order to compare the elements spatial co-occurrences and correlations, tricolor (Ce, Mn and Ca) composite maps and Ce-Mn frequency plots of a pinna are provided in Fig. S6. The results further confirm the co-localization of Ce and Mn both inside and outside the necrotic lesions, with higher concentrations inside the necrotic lesions and lower outside. However, tri-color elemental maps and element association frequency plots also show that Ce and Mn are not totally co-localised, *e.g.* the

214 highly concentrated Ce areas at the lamina between two pinnules (Fig. S6), have relatively low Mn
215 concentrations.
216
217 **Localization of REEs in pinnule and midvein cross-sections.** In order to establish the localization
218 of REEs at the cellular level, XFM mapping was performed on cross-sections of midvein and
219 pinnule. The elemental maps revealed that La + Ce and Mn are co-localised in the epidermis (Fig. 3;
220 Fig. 4). The La + Ce and Mn in the upper epidermis are much more concentrated than in the low
221 epidermis. In the midvein cross-section (Fig. 4), there is a "ring" shaped peak of La + Ce and Mn
222 between the vascular bundle and the cortex, likely the pericycle. In the pinnule cross-section (Fig. 3),
223 the vascular bundle and cortex are difficult to differentiate. However, compared to La + Ce, Mn
224 signals are more prominent in the cortex and mesophyll, while less marked in the vascular bundle.
225 Potassium is low in the cortex, but concentrated in the mesophyll, epidermis and vascular bundle.
226 Calcium is predominantly localised in the mesophyll and epidermis, but low in the vascular bundle
227 and cortex. The subcellular elemental distribution could not be differentiated for any element.
228
229 **Localization of REEs in rachis and stolon cross-sections.** The elemental XFM maps of the rachis
230 and stolon cross-sections show La + Ce enrichment in the epidermis and vascular bundle, while in
231 the cortex and the pericycle of the rachis cross-sections prevailing concentrations are very low (Fig.
232 S7; Fig. S8). In contrast, in both the rachis and stolon cross-sections, the K, Ca and Mn are similar
233 and mostly concentrated in the epidermis, pericycle and vascular bundle, with distinct localizations

234 in the cortex. Within the vascular bundle of rachis cross-sections, La + Ce, Mn, K and Ca are mainly
235 localised in the protoxylem and metaxylem.
236
237 **DISCUSSION**
238 *Dicranopteris linearis* accumulates up to 0.2% total REEs in the shoots or 0.5% in the dead standing
239 litter of pinnae, much higher than the other 20 potential REE (hyper)accumulator plants known
240 globally (Table S3). The fact that *D. linearis* accumulates such high REEs concentrations in its
241 aboveground parts while growing on REE mine tailings (Table S1), shows that this pioneer fern can
242 successfully adapt to REE mine tailings, and this infers potential for use in phytotechnological
243 applications. *Dicranopteris linearis* accumulates the highest concentrations of REEs in necrotic
244 lesions (Fig. 2), which differs significantly from the behavior of most other metal hyperaccumulators.
245 The markedly higher concentrations of REEs, Al and Si in the dead standing litter of pinnae, as
246 compared to the live pinnae further affirms that these elements are rather immobile as opposed to K
247 which is strongly depleted in litter tissues (Table 1). The concentrations of Mn in the pinnae of *D.*
248 *linearis* (1480 ± 523 mg kg^{-1}, Table 1) are much greater than what is typically toxic in most of the
249 plants (*e.g.* <200 mg kg^{-1} in maize or 275 ± 659 mg kg^{-1} in various species of naturally grown ferns)
250 (36, 37). Therefore, the necrosis in these tissues is possibly, among other reasons, the result of Mn
251 accumulation, oxidation and localised toxicity within the pinnules, which then induces cell death,
252 necrotic spots, substantially larger necrotic lesion and then finally acts as a 'dump site' for REEs as a
253 result of cells damage, higher evaporation rate and transpiration flow. A similar phenomenon has
254 been reported in the leaves of soybean and cowpea in response to Mn toxicity; the toxicity started

255 with Mn pumped under the cuticle *via* the apoplast, or Mn is expelled *via* hydathodes towards the
256 leaf tip, and then increasing concentrations of Mn leading to Mn oxidation (+2 to +3 and +4
257 valences) and the formation of necrotic lesions, which in turn stimulate more Mn translocation as a
258 result of higher evaporation (38, 39). However, Ce and Mn were not totally co-localised, it is
259 therefore also possible that the necrotic lesions were induced by Ce accumulation and oxidation (+3
260 to +4 valences). It could be also interpreted as a tolerance mechanism in which some cells are
261 sacrificed and used as a dump, while in the others, photosynthesis and normal activity can continue
262 (40). The underlying mechanisms as to why REEs prefer to compartmentalize into the upper
263 epidermis, margins and veins are not fully understood. Previous studies on hyperaccumulator plants
264 suggest that it may reflect a physiological and/or defense-related response – protection of
265 photosynthetically active tissues such as mesophyll, and defense from predation by herbivores and
266 pathogens (41, 42).
267
268 The distinct localization in vascular bundles, while prevailing concentrations are low in the cortex of
269 rachis and midvein (Fig. 4; Fig. S7), suggests an efficient REE transport system in this plant. The
270 transport of REEs to the pinnules probably occurs as mass flow through the vascular tissue, driven
271 by transpiration. In non-accumulating species of beech and oak (Fagaceae), REEs transport within
272 xylem was suggested to be associated with general nutrient flux (43). However, in the vascular
273 bundles of *D. linearis*, a small area of La + Ce peaks within vascular bundle and a very bright “ring”
274 shaped peak between vascular bundle and cortex was observed (Fig. 4). The significant La + Ce
275 enrichment, with no obvious Ca and Mn enrichment within the vascular bundle of veins, suggests

276 that REEs are translocated to the blade to a lesser extent than Ca and Mn. This might be due to the
277 features of the pericycle tissue where cells are dense, preventing REEs translocation from the xylem
278 into the pinnules *via* the intercellular space. It is possible that once the REEs enter into the vascular
279 system of veins (xylem), they are partly fixed by the pericycle, and then transported to the *D. linearis*
280 pinnules (especially to the epidermis and necrotic lesions) *via* transpiration flow. In this case, the
281 transport and accumulation of REEs is likely to be passive convection processes. Thus, the
282 distribution of REEs in *D. linearis* pinnules could be influenced by various parameters that are
283 associated with the evaporation (*e.g.* habitat, seasonal and climatic conditions) and Mn toxicity (*e.g.*
284 light intensity, pinnule age and height at sampling) (44–46). The highest concentrations of REEs are
285 recorded within the necrotic lesions of pinna which may be ascribed to a lack of wax coats at the
286 surface of pinna, and/or the damage of the pericycle tissue or cells between vascular bundle and
287 cortex in the veins, thus leading to a higher evaporation rate. The higher evaporation rate may also
288 lead to higher concentrations of REEs in the upper epidermis, compared to the lower epidermis (Fig.
289 3; Fig. 4).
290
291 As vacuoles in necrotic lesions of the pinnae disintegrate, compartmentalization and accumulation in
292 these areas suggest that the REEs are likely to be sequestrated by cell walls or exist under immobile
293 forms. Many studies found that REEs tend to complex with phosphate and form deposits in the cell
294 walls and more generally in the intercellular space of plant tissues (47). However, the molar ratio of
295 P in *D. linearis* pinnae was much lower than that of the REEs (Table 1). Moreover, we found that *D.*
296 *linearis* also accumulates high concentration of Al and Si. Detoxification of Al and other heavy

297 metals by Si has been reported for many plants (48). For example, Al localization coincided with Si
298 distribution in cell walls of the Al hyperaccumulator *Rudgea viburnoides* (49), and the co-deposition
299 of Si and Cd in the cell walls as a [Si-wall matrix]Cd co-complex inhibited Cd ion uptake by rice cell
300 (50). In the Al and Si hyperaccumulator *Faramea marginata*, Al and Si are thought to be co-
301 deposited as phytolith (silicon oxides) Al (51). Also, silicon may co-deposit with Mn at the apoplast
302 and decrease the oxidation of Mn in cowpea, soybean and sunflower (38). In a previous study,
303 numerous particles (phytolith and phytolith Al) were detected at the upper epidermis of *D. linearis*
304 pinnules (29). Rare earth elements are a group of trivalent elements, which exhibit many chemical
305 similarities to Al (52). Considering the high concentrations of Si, a co-deposition of REEs, Mn and
306 Al with Si may be involved in the physiological regulation of high concentrations of REEs, Mn and
307 Al in *D. linearis*.
308
309 **AUTHOR CONTRIBUTIONS**
310 WSL conducted the fieldwork and collected the samples. AvdE, GE, PDE, KMS and KMS
311 conducted the synchrotron XFM experiment. KMS, AvdE and EMP performed the XFM data
312 processing and analysis. WSL conducted bulk elemental analysis. All authors contributed to writing
313 the manuscript.
314
315 **ACKNOWLEDGEMENTS**
316 This work was financially supported by the National Natural Science Foundation of China
317 (41771343), and the 111 Project (B18060). Parts of this research were carried out at P06 at DESY, a

member of the Helmholtz Association (HGF). The research leading to this result has been supported by the project CALIPSOplus under the Grant Agreement 730872 from the EU Framework Programme for Research and Innovation HORIZON 2020. The French National Research Agency through the national "Investissements d'avenir" program (ANR-10-LABX-21, LABEX RESSOURCES21) and through the ANR-14-CE04-0005 Project "Agromine" is acknowledged for funding support.

SUPPORTING INFORMATION

Dicranopteris linearis growing on ion-adsorption REE mine tailings; synchrotron-based X-ray fluorescence microscopy elemental maps of hydrated *D. linearis* pinna, pinnules, and cross-sections of rachis and stolon; tri-color elemental maps (Ce, Mn and Ca) in a pinna and element association (Ce and Mn) frequency plots; REEs concentrations in *D. linearis* and rhizosphere soil samples collected from different sites; REEs concentrations of live *D. linearis* pinnae and dead standing litter of pinnae; REEs concentrations in the shoots of (hyper)accumulator plants.

REFERENCES

(1) Binnemans, K.; Jones, P. T.; Blanpain, B.; Gerven, T. V.; Yang, Y.; Walton, A.; Buchert, M. Recycling of rare earths: a critical review. *J. Clean. Prod*. **2013**, *51*, 1–22.

(2) Migaszewski, Z. M.; Gałuszka, A. The characteristics, occurrence, and geochemical behavior of rare earth elements in the environment: a review. *Crit. Rev. Environ. Sci. Technol.* **2015**, *45*, 429–471.

(3) Redling, K. Rare earth elements in agriculture with emphasis on animal husbandry. Ludwig-Maximilians-Universität München. **2006**.

(4) Wang, L. H.; Li, J. G.; Zhou, Q.; Yang, G. M.; Ding, X. L.; Li, X. D.; Cai C. X.; Zhang Z.; Wei H. Y.; Lu, T. H.; Deng, X. W.; Huang X. H. Rare earth elements activate endocytosis in plant cells. *Proc. Natl. Acad. Sci. U. S. A.* **2014**, *111*, 12936–12941.

(5) Baker, A. J. M.; Brooks, R. R. Terrestrial higher plants which hyper accumulate metallic elements. *Biorecovery*. **1989**, *1*, 81–126.

(6) Reeves, R. D. Tropical hyperaccumulators of metals and their potential for phytoextraction. *Plant Soil*. **2003**, *249*, 57–65.

(7) van der Ent, A.; Baker, A. J. M.; Reeves, R. D.; Pollard, A. J.; Schat, H. Hyperaccumulators of metal and metalloid trace elements: facts and fiction. *Plant Soil*. **2013**, *362*, 319–334.

(8) Reeves, R. D.; van der Ent, A.; Baker, A. J. M. Agromining: farming for metals. In *Global distribution and ecology of hyperaccumulator plants*; van der Ent, A.; Echevarria, G.; Baker, A. J. M.; Morel, J. L.; eds.; Mineral Resource Reviews series, Cham: Springer International Publishing. **2018**; pp. 75–92.

(9) Liu, C.; Yuan, M.; Liu, W. S.; Guo, M. N.; Huot, H.; Tang, Y. T.; Laubie, B.; Simonnot, M. O.; Morel, J. L.; Qiu, R. L. Agromining: farming for metals. In *Element case studies: rare earth elements*; van der Ent, A.; Echevarria, G.; Baker, A. J. M.; Morel, J. L.; eds.; Mineral Resource Reviews series, Cham: Springer International Publishing. **2018**; pp. 297–308.

(10) Wei, Z. G.; Zhang, H. J.; Li, H. X.; Hu, F. Research trends on rare earth element hyperaccumulator. *J. Chin. Rare Earth Soc*. **2006**, *24*, 1–11. (in Chinese)

(11) van der Ent, A.; Baker, A. J. M.; Reeves, R. D.; Chaney, R. L.; Anderson, C. W. N.; Meech, J. A.; Erskine, P. D.; Simonnot, M. O.; Vaughan, J.; Morel, J. L.; Echevarria, G.; Fogliani, B.; Qiu, Q. L.; Mulligan, D. R. Agromining: farming for metals in the future? *Environ. Sci. Technol.* **2015**, *49*, 4773–4780.

(12) Tappero, R.; Peltier, E.; Gräfe, M.; Heidel, K.; Ginder-Vogel, M.; Livi, K. J. T.; Rivers, M. L.; Marcus, M. A.; Chaney, R. L.; Sparks, D. L. Hyperaccumulator *Alyssum murale* relies on a different metal storage mechanism for cobalt than for nickel. *New Phytol*. **2007**, *175*, 641–654.

(13) Tian, S. K.; Lu, L. L.; Yang, X. E.; Labavitch, J. M.; Huang, Y. Y.; Brown, P. Stem and leaf sequestration of zinc at the cellular level in the hyperaccumulator *Sedum alfredii*. *New Phytol.* **2009**, *182*, 116–126.

(14) Hu, P. J.; Wang, Y. D.; Przybyłowicz, W. J.; Li, Z.; Barnabas, A.; Wu, L. H.; Mesjasz-Przybyłowicz, J. Elemental distribution by cryo-micro-PIXE in the zinc and cadmium hyperaccumulator *Sedum plumbizincicola* grown naturally. *Plant Soil*. **2015**, *388*, 267–282.

(15) Hokura, A.; Omuma, R.; Terada, Y.; Kitajima, N.; Abe, T.; Saito, H.; Yoshida, S.; Nakai, I. Arsenic distribution and speciation in an arsenic hyperaccumulator fern by x-ray spectrometry utilizing a synchrotron radiation source. *J. Anal. At. Spectrom.* **2006**, *21*, 321–328.

(16) Li, J. T.; Gurajala, H. K.; Wu, L. H.; van der Ent, A.; Qiu, R. L.; Baker, A. J.; Tang, Y. T.; Yang, X. E.; Shu, W. S. Hyperaccumulator plants from China: A synthesis of the current state of knowledge. *Environ. Sci. Technol.* **2018**, *52*, 11980–11994.

(17) Zhao, F. J.; Moore, K. L.; Lombi, E.; Zhu, Y. G. Imaging element distribution and speciation in plant cells. *Trends Plant Sci.* **2014**, *19*, 183–192.

(18) van der Ent, A.; Przybyłowicz, W. J.; de Jonge, M. D.; Harris, H. H.; Ryan, C. G.; Tylko, G.; Paterson, D. J.; Barnabas, A. D.; Kopittke, P. M.; Mesjasz-Przybyłowicz, J. X-ray elemental mapping techniques for elucidating the ecophysiology of hyperaccumulator plants. *New Phytol.* **2018**, *218*, 432–452.

(19) Sharma, S. S.; Dietz, K.; Mimura, T. Vacuolar compartmentalization as indispensable component of heavy metal detoxification in plants. *Plant Cell Environ.* **2016**, *39*, 1112–1126.

(20) Nieboer, E.; Richardson, H. S. The replacement of the nondescript term 'heavy metals' by a biologically and chemically significant classification of metal ions. *Environ. Pollut. Ser. B*. **1980**, *1*, 3–26.

(21) Russell, A. E.; Raich, J. W.; Vitousek, P. M. The ecology of the climbing fern *Dicranopteris linearis*, on windward Mauna Loa, Hawaii. *J. Ecol*. **1998**, *86*, 765–779.

(22) Chen, Z. Q.; Chen, Z. B.; Yan, X. Y.; Bai, L. Y. Stoichiometric mechanisms of *Dicranopteris dichotoma*, growth and resistance to nutrient limitation in the Zhuxi watershed in the red soil hilly region of China. *Plant Soil*. **2016**, *398*, 367–379.

(23) Shan, X. Q.; Wang, H. O.; Zhang, S. Z.; Zhou, H. F.; Zheng, Y.; Yu, H.; Wen, B. Accumulation and uptake of light rare earth elements in a hyperaccumulator *Dicropteris dichotoma*. *Plant Sci.* **2003**, *165*, 1343–1353.

(24) Wei, Z. G.; Hong, F. S.; Yin, M.; Li, H. X.; Hu, F.; Zhao, G. W.; Wong, W. J. Subcellular and molecular localization of rare earth elements and structural characterization of yttrium bound chlorophyll a in naturally grown fern *Dicranopteris dichotoma*. *Microchem. J*. **2005**, *80*, 1–8.

(25) Lombi, E.; Susini, J. Synchrotron-based techniques for plant and soil science: opportunities, challenges and future perspectives. *Plant Soil*. **2009**, *320*, 1–35.

(26) Kopittke, P. M.; Punshon, T.; Paterson, D. J.; Tappero, R. V.; Wang, P.; Blamey, F. P. C.; van der Ent, A.; Lombi, E. Synchrotron-based X-ray fluorescence microscopy as a technique for imaging of elements in plants. *Plant Physiol*. **2018**, *178*, 507–523.

(27) James. S.; van der Ent, A.; Harris, H. H. Tracking metal ions in biology using X-ray methods. *Encycl. Inorg. Bioinorg. Chem.* **2019**, https://doi.org/10.1002/9781119951438.eibc2692.

(28) Chao, Y. Q.; Liu, W. S.; Chen, Y. M.; Chen, W. H; Zhao, L. H.; Ding, Q. B.; Wang, S. Z.; Tang, Y. T.; Zhang, T; Qiu, R. L. Structure, variation, and co-occurrence of soil microbial communities in abandoned sites of a rare earth elements mine. *Environ. Sci. Technol*. **2016**, *50*, 11481–11490.

412 (29) Liu, W. S.; Zheng, H. X.; Guo, M. N.; Liu, C.; Huot, H.; Morel, J. L.; van der Ent, A.; Tang, Y.
413 T.; Qiu, R. L. Co-deposition of silicon with rare earth elements (REEs) and aluminium in the
414 fern *Dicranopteris linearis* from China. *Plant Soil*. **2019**, *437*, 427–437.
415 (30) Boesenberg, U.; Ryan, C. G.; Kirkham, R.; Siddons, D. P.; Alfeld, M.; Garrevoet, J.; Núñez, T.;
416 Claussen, T.; Kracht, T.; Falkenberg, G. Fast X-ray microfluorescence imaging with
417 submicrometer-resolution integrating a Maia detector at beamline P06 at PETRA III. *J.*
418 *Synchrotron Radiat.* **2016**, *23*, 1550−1560.
419 (31) Ryan, C. G.; Kirkham, R.; Hough, R. M.; Moorhead, G.; Siddons, D. P.; de Jonge, M. D.;
420 Paterson, D. J.; de Geronimo, G.; Howard, D. L.; Cleverley, J. S. Elemental X-ray imaging using
421 the Maia detector array: the benefits and challenges of large solid-angle. *Nucl. Instr. Methods*
422 *Phys. Res*. *A*. **2010**, *619*, 37–43.
423 (32) Ryan, C. G.; Kirkham, R.; de Jonge, M. D.; Siddons, D. P.; van der Ent, A.; Pagès, A.;
424 Boesenberg, U.; Kuczewski, A. J.; Dunn, P.; Jensen, M.; Liu, W.; Harris, H. H.; Moorhead, G.
425 F.; Paterson, D. J.; Howard, D. L.; Afshar, N.; Garrevoet, J.; Spiers, K.; Falkenberg, G.; Woll, A.
426 R.; De Geronimo, G.; Carini, G. A.; James, S. A.; Jones, M. W. M.; Fisher, L. A.; Pearce, M.
427 The Maia detector and event mode. *Synchrotron News*. **2018**, *31*, 21–27.
428 (33) Jones, M. W. M.; Kopittke, P. M.; Casey, L. W.; Reinhardt, J.; Blamey, F. P. C.; van der Ent, A.
429 Assessing radiation dose limits for X-ray fluorescence microscopy analysis of plant specimens.
430 *Ann. Bot.* **2019**, https://doi.org/10.1093/aob/mcz195.
431 (34) Ryan, C. G. Quantitative trace element imaging using PIXE and the nuclear microprobe. *Int. J.*
432 *Imag. Sys. Technol*. **2000**, *11*, 219–230.
433 (35) Ryan, C. G.; Achterbergh, E. V.; Jamieson, D. N. Advances in dynamic analysis, PIXE imaging:
434 correction for spatial variation of pile-up components. *Nucl. Instru. Methods Phys. Res*. **2005**,
435 *231*, 162–169.
436 (36) Shao, J. F.; Yamaji, N.; Shen, R. F.; Ma, J. F. The key to Mn homeostasis in plants: regulation of
437 Mn transporters. *Trends Plant Sci.* **2017**, *22*, 215–224.

438 (37) Schmitt, M.; Mehltreter, K.; Sundue, M.; Testo, W.; Watanabe, T.; Jansen, S. The evolution of
439 aluminum accumulation in ferns and lycophytes. *Am J Bot*. **2017**, *104*, 573–583.
440 (38) Blamey, F. P. C.; Mckenna, B. A.; Li, C.; Cheng, M. M.; Tang, C. X.; Jiang, H. B.; Howard, D.
441 L.; Paterson, D. J.; Kappen, P.; Wang, P.; Menzies, N. W.; Kopittke, P. M. Manganese
442 distribution and speciation help to explain the effects of silicate and phosphate on manganese
443 toxicity in four crop species. *New Phytol*. **2018a**, *217*, 1146–1160.
444 (39) Blamey, F. P. C.; Paterson, D. J.; Walsh, A.; Afshar, N.; McKenna, B. A.; Cheng, M. M.; Tang,
445 C. X.; Horst, W. J.; Menzies, N. W.; Kopittke, P. M. Time-resolved X-ray fluorescence analysis
446 of element distribution and concentration in living plants: An example using manganese toxicity
447 in cowpea leaves. *Environ. Expe. Bot*. **2018b**, *156*, 151–160.
448 (40) Küpper, H.; Parameswaran, A.; Leitenmaier, B.; Trtílek, M.; Šetlík, I. Cadmium-induced
449 inhibition of photosynthesis and long-term acclimation to cadmium stress in the
450 hyperaccumulator *Thlaspi caerulescens*. *New Phytol*. **2007**, *175*, 655–674.
451 (41) Martens, S. N.; Boyd, R. S. The ecological significance of nickel hyperaccumulation: a plant
452 chemical defense. *Oecologia*. **1994**, *98*, 379–384.
453 (42) Cappa, J. J.; Pilon-Smits, E. A. Evolutionary aspects of elemental hyperaccumulation. *Planta*.
454 **2014**, *239*, 267–275.
455 (43) Brioschi, L.; Steinmann, M.; Lucot, E.; Pierret, M. C.; Stille, P.; Prunier, J.; Badot, P. M.
456 Transfer of rare earth elements (REE) from natural soil to plant systems: implications for the
457 environmental availability of anthropogenic REE. *Plant Soil*. **2013**, *366*, 143–163.
458 (44) Küpper, H.; Mijovilovich, A.; Meyerklaucke, W.; Kroneck, P. M. H. Tissue- and age-dependent
459 differences in the complexation of cadmium and zinc in the cadmium/zinc hyperaccumulator
460 *Thlaspi caerulescens* (Ganges ecotype) revealed by X-ray absorption spectroscopy. *Plant*
461 *Physiol*. **2004**, *134*, 748–757.
462 (45) Bartoli, F.; Royer, M.; Coinchelin, D.; Thiec, D. L.; Rose, C.; Robin, C.; Echevarria, G.
463 Multiscale and age-dependent leaf nickel in the Ni-hyperaccumulator *Leptoplax emarginata*.
464 *Ecol. Res*. **2018**, *33*, 1–14.

(46) Fernando, D. R.; Lynch, J. P. Manganese phytotoxicity: new light on an old problem. *Ann. Bot.* **2015**, *116*, 313–319.

(47) Ding, S. M.; Liang, T.; Zhang, C. S.; Huang, Z. C.; Xie, Y. N; Chen, T. B. Fractionation mechanisms of rare earth elements (REEs) in hydroponic wheat: an application for metal accumulation by plants. *Environ. Sci. Technol.* **2006**, *40*, 2686–2691.

(48) Liang, Y.; Sun, W.; Zhu, Y. G.; Christie, P. Mechanisms of silicon-mediated alleviation of abiotic stresses in higher plants: a review. *Environ. Pollut*. **2007**, *147*, 422–428.

(49) Malta, P. G.; Arcanjo-Silva, S.; Ribeiro, C.; Campos, N. V.; Azevedo, A. A. *Rudgea viburnoides* (Rubiaceae) overcomes the low soil fertility of the Brazilian Cerrado and hyperaccumulates aluminum in cell walls and chloroplasts. *Plant Soil*. **2016**, *408*, 369–384.

(50) Liu, J.; Ma, J.; He, C. W.; Li, X. L.; Zhang, W. J.; Xu, F. S.; Lin, Y. J.; Wang, L. J. Inhibition of cadmium ion uptake in rice (*Oryza sativa*) cells by a wall-bound form of silicon. *New Phytol.* **2013**, *200*, 691–699.

(51) Britez, R. M.; Watanabe, T.; Jansen, S.; Reissmann, C. B.; Osaki, M. The relationship between aluminium and silicon accumulation in leaves of *Faramea marginata* (Rubiaceae). *New Phytol.* **2002**, 156, 437–444.

(52) Pletnev, I. V.; Zernov, V. V. Classification of metal ions according to their complexing properties: a data-driven approach. *Anal. Chim. Acta.* **2002**, *455*, 131–142.

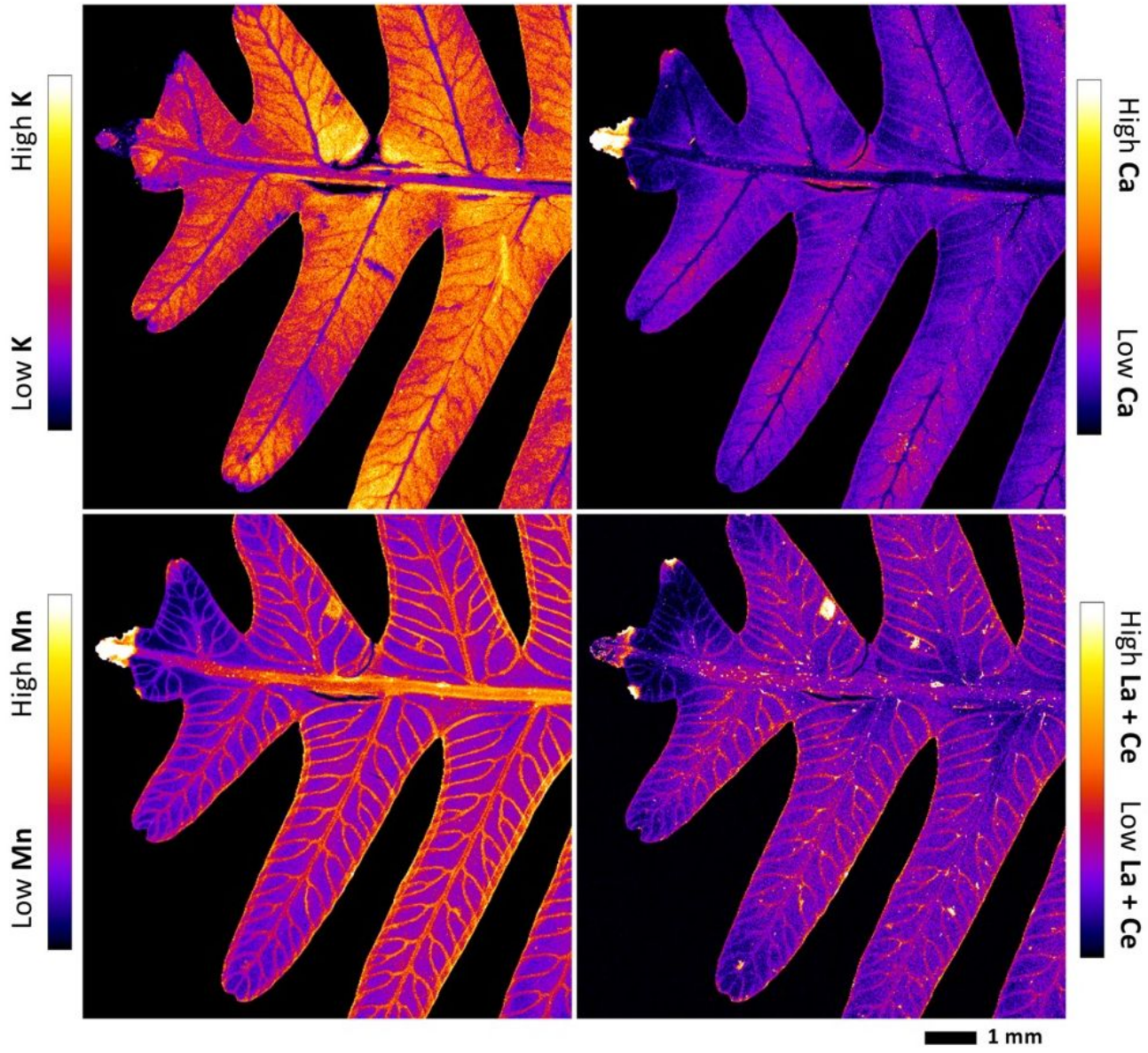

Fig. 1. Synchrotron-based X-ray fluorescence microscopy elemental maps of a hydrated *Dicranopteris linearis* pinna. The maps measure 8.86 × 8.56 mm. The elemental image was acquired with a step size of 15 μm with a dwell of 15 ms per pixel using a 12.0 keV incident beam.

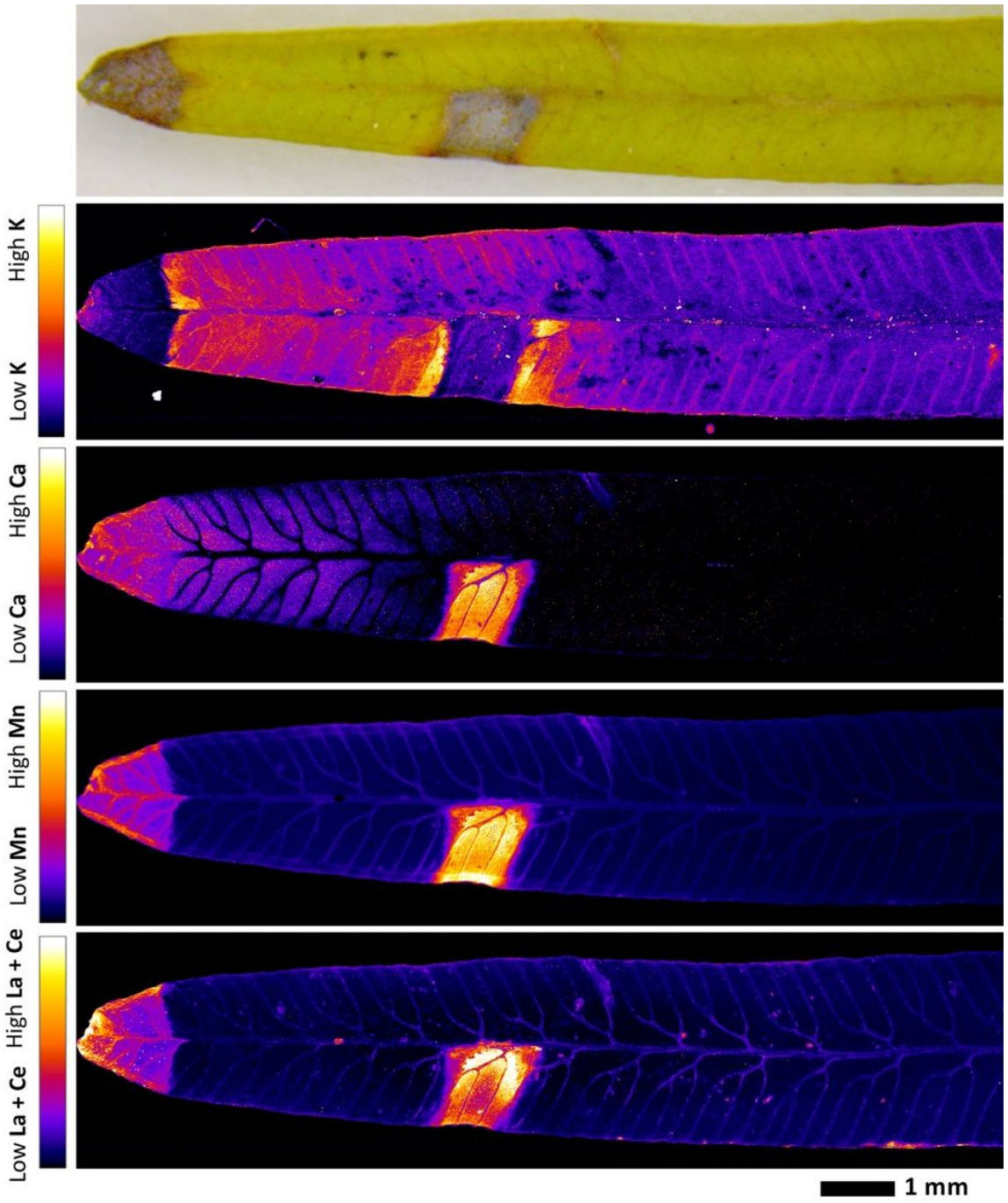

Fig. 2. Synchrotron-based X-ray fluorescence microscopy elemental maps of a hydrated *Dicranopteris linearis* pinnule. The maps measure 12.95 × 2.88 mm. The elemental image was acquired with a step size of 8 µm with a dwell of 15 ms per pixel using a 12.0 keV incident beam.

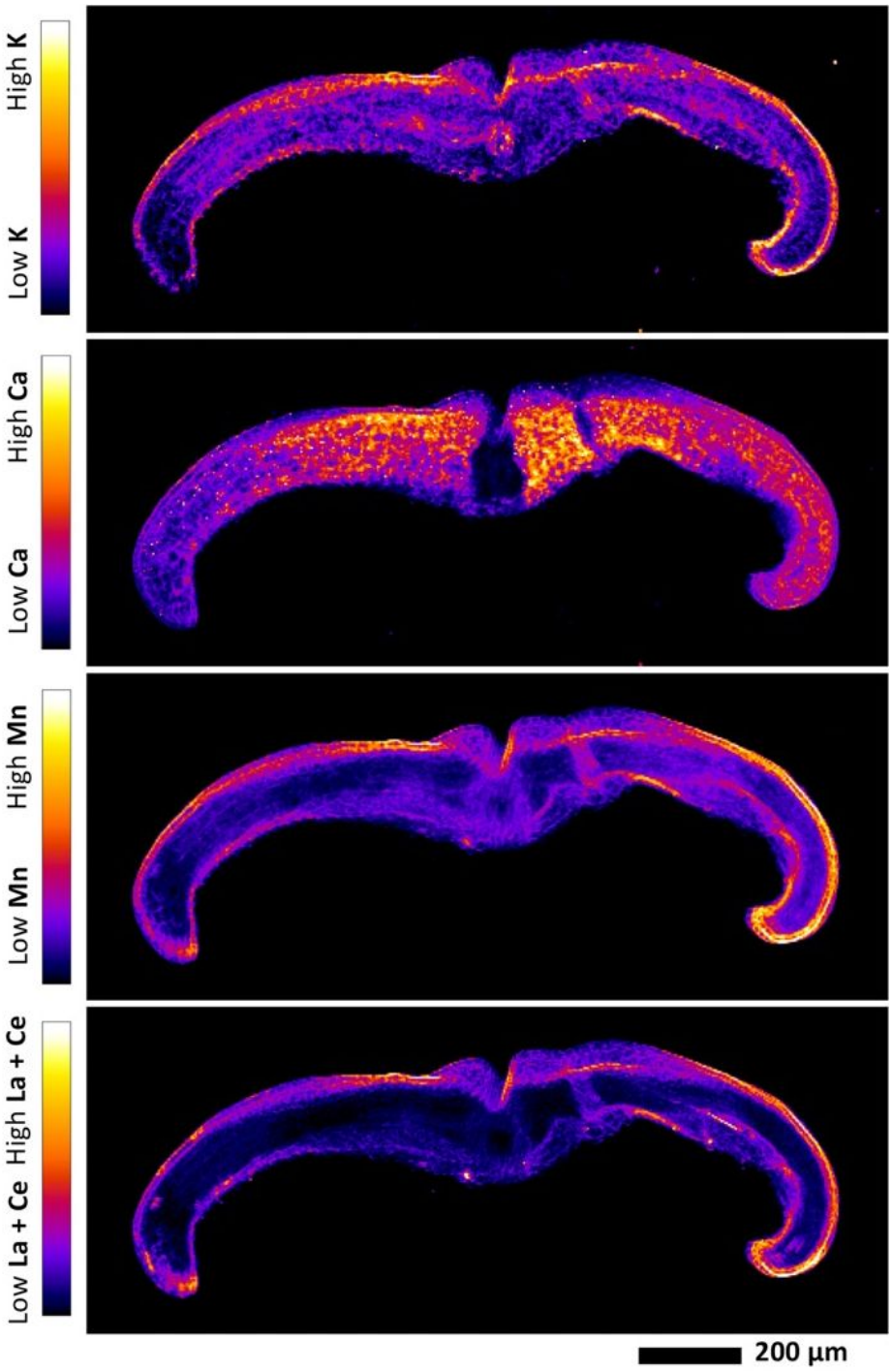

Fig. 3. Synchrotron-based X-ray fluorescence microscopy elemental maps of a hydrated *Dicranopteris linearis* pinnule cross-section. The maps measure 2.25 × 0.86 mm. The elemental image was acquired with a step size of 5 µm with a dwell of 15 ms per pixel using a 12.0 keV incident beam.

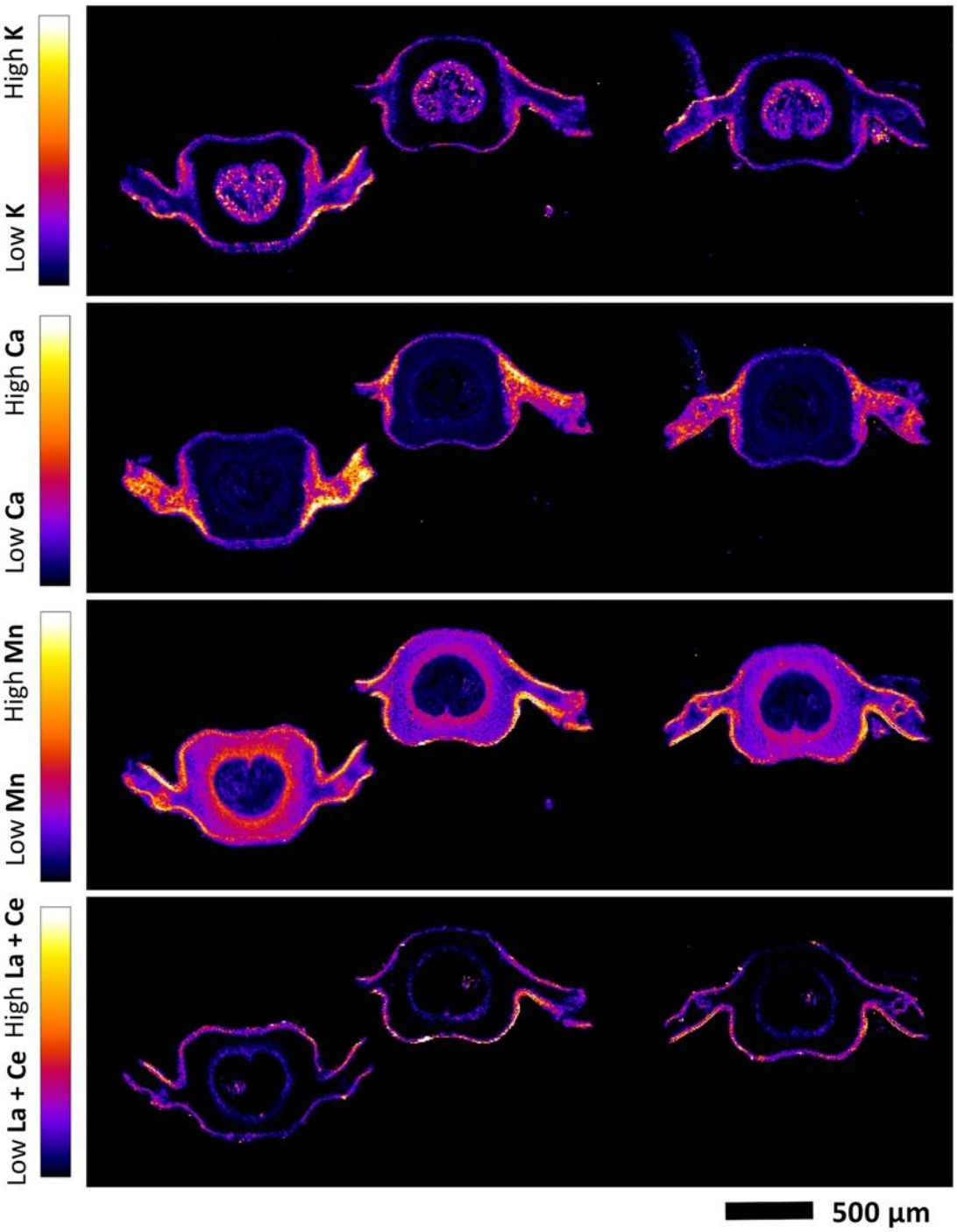

Fig. 4. Synchrotron-based X-ray fluorescence microscopy elemental maps of hydrated *Dicranopteris linearis* midvein cross-sections of pinna. The maps measure 4.70 × 1.57 mm. The elemental image was acquired with a step size of 8 µm with a dwell of 15 ms per pixel using a 12.0 keV incident beam. The concave side represents the adaxial side in the figure.

507 **TABLES**

508

509 **Table 1.** Bulk elemental concentrations in live and dead standing litter of pinnae of *Dicranopteris*
510 *linearis* (mg kg^{-1} dry weight).

511

Type	Al	Si	REEs*	La + Ce	Ca	Mn	P	K
Living pinnae	2850±997 a	14700±3310 a	1900±505 a	1040±520 a	1810±676 a	1480±523 b	211±23.0 b	3000±413 b
Standing litter pinnae	4850±455 b	33900±4910 b	3500±327 b	1980±317 a	1400±779 a	310±205 a	129±28.0 a	268±152 a

512

513 * *The summed concentrations of La, Ce, Pr, Nd, Sm, Eu, Gd, Tb, Dy, Ho, Er, Tm, Yb, Lu and Y, see*
514 *the concentration of each rare earth element in Table S2. Different letters in the table represent*
515 *significant difference among each group (ANOVA, Duncan, $p<0.05$).*